CHEMISTRY
A EUROPEAN JOURNAL

DOI: 10.1002/chem.200601116

Neutron Powder Diffraction with ^{nat}Sm: Crystal Structures and Magnetism of a Binary Samarium Deuteride and a Ternary Samarium Magnesium Deuteride

Holger Kohlmann,*[a] Franz Werner,[b] Klaus Yvon,[b] Gerfried Hilscher,[c] Michael Reissner,[c] and Gabriel J. Cuello[d]

Abstract: Binary SmH_3 (trigonal, $a=656.7(3)$, $c=680.1(3)$ pm, $P\bar{3}c1$, $Z=6$), ternary $SmMg_2H_7$ (tetragonal, $a=626.47(6)$, $c=937.2(2)$ pm, $P4_12_12$, $Z=4$) and the corresponding deuterides SmD_3 ($a=653.9(1)$m, $c=676.7(2)$ pm) and $SmMg_2D_7$ ($a=624.10(1)$, $c=934.81(2)$ pm) have been prepared by hydrogenation (deuteration) of elemental samarium and the Laves phase $SmMg_2$, respectively, and investigated by X-ray and neutron powder diffraction and SQUID and vibration magnetometry. The problem of the enormous neutron absorption of the natural isotopic mixture (^{nat}Sm) is circumvented by carefully choosing the neutron wavelength (≈ 50 pm) and the use of double-walled cylindrical sample holders and a high-intensity neutron diffractometer (D4c at ILL). SmD_3 crystallises with a tysonite-type structure and has three independently ordered deuterium atom sites with trigonal-planar, trigonal-pyramidal and tetrahedral metal environments and Sm–D bond lengths in the range 220(1)–258(1) pm (average: 235 pm). $SmMg_2D_7$ is a new deuteride that crystallises with an $LaMg_2D_7$-type structure. It displays four fully occupied deuterium sites having triangular and tetrahedral metal environments and Sm–D bond lengths in the range 227.6(5)–246.8(8) pm (average: 239 pm). These are the first samarium–deuterium bond lengths to be reported. Both deuterides are paramagnetic down to 2 K (SmD_3: $\mu_{eff}=0.63(1)\,\mu_B$, $\theta_p\approx -4$ K; $SmMg_2D_7$: $\mu_{eff}=0.57(2)\,\mu_B$, $\theta_p\approx -4$ K). Their crystal structures and chemical and physical properties suggest mainly ionic bonding according to the limiting ionic formulae $Sm^{3+}(H^-)_3$ and $Sm^{3+}(Mg^{2+})_2(H^-)_7$.

Keywords: crystal structures · deuterium · hydrides · magnetism · neutron absorption · samarium

Introduction

Rare-earth-containing metal hydrides are often constituents of hydrogen storage materials,[1] and this has prompted renewed interest in the basic properties of binary lanthanide (Ln) hydrides (for a review see reference [2] and references therein) and ternary metal hydrides based on lanthanides and light metals such as magnesium (for a recent review see reference [3]). A large variety of hydride compositions have been investigated with respect to hydrogen (deuterium) atom distributions (e.g. $LaD_{2.47}$,[4] CeD_3,[5] $PrD_{2.92}$,[6] NdD_3[7]) and magnetic properties[2] for the lighter lanthanides (La–Nd). The hydrides of the heavier lanthanides, however, are less well studied. This is particularly true for samarium hydride phases, which have been known since 1955[8] but whose structures and magnetism have still not been fully characterised. The compressibility and structure of the cubic SmH_2 phase have been studied by neutron powder diffraction for a deuteride of the ^{154}Sm isotope,[9] although reliable

[a] Dr. H. Kohlmann
FR. 8.1 Anorganische und Analytische Chemie
Universität des Saarlandes
Postfach 15 11 50, 66041 Saarbrücken (Germany)
Fax: (+49) 681-302-4233
E-mail: h.kohlmann@mx.uni-saarland.de

[b] Dr. F. Werner, Prof. Dr. K. Yvon
Laboratoire de Cristallographie
Université de Genève
Quai E. Ansermet 24, 1211 Genève 4 (Switzerland)

[c] Prof. Dr. G. Hilscher, Prof. Dr. M. Reissner
Technische Universität Wien
Institut für Festkörperphysik
Wiedner Hauptstraße 8–10/138, 1040 Wien (Austria)

[d] Dr. G. J. Cuello
Institut Laue-Langevin
6, Rue Jules Horowitz, BP 156, 38042 Grenoble Cedex 9 (France)

samarium–deuterium bond distances for this fluorite-type structure have not been reported. As for the trigonal hydride phase SmH_3, old X-ray data suggest a trigonal HoD_3-like structure,[10] although no refined metal atom positions were given and the hydrogen (deuterium) positions were not determined. No samarium analogue of the recently reported ternary hydrides of lanthanides and magnesium ($LnMg_2D_7$; Ln = La, Ce)[11] is known as yet. We report here the structural and magnetic properties of SmD_3 and compare them to those of the new ternary samarium-magnesium deuteride $SmMg_2H_7$.

To the best of our knowledge no full structure determination of any samarium hydride has been reported in the literature to date. This is probably due to the enormous neutron absorption of samarium (Figure 1), which would appear to make neutron diffraction studies unfeasible. However, we demonstrate in this paper how to circumvent this problem for samarium hydrides (deuterides) containing the natural isotopic mixture of samarium by carefully optimising the parameters of the neutron powder diffraction experiment, similar to the strategy used during the investigation of europium and cadmium hydrides,[12–15] and thus present the first complete crystal structures of samarium deuterides and the first reliable Sm–D bond lengths.

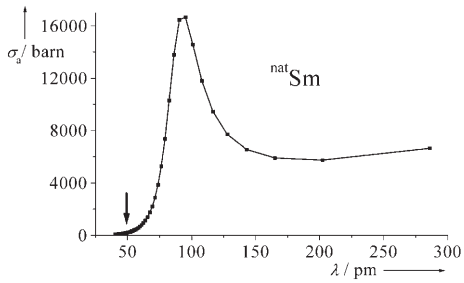

Figure 1. Wavelength-dependence of the neutron absorption cross-section of natural samarium, σ_a (^{nat}Sm), as calculated by $\sigma_a = 4\pi/kb''_c$ (k = norm of the neutron radiation wave vector; b''_c = imaginary part of the bound coherent scattering length, taken from [16]). The wavelength used for the neutron diffraction experiment (49.4 pm) is marked by an arrow.

Results

The X-ray diffraction patterns for $SmH(D)_3$ were indexed to a hexagonal cell (Table 1) and the proposed HoD_3-type structure[17] was used as a starting model for the crystal structure refinement. The lattice parameter of cubic Laves phase (C15)-type $SmMg_2$ was refined from the X-ray powder diffraction data by the Rietveld method. In agreement with a literature report,[18] this compound shows a slight non-stoichiometry that is dependent on the synthesis

Table 1. Cell parameters, properties, experimental conditions and refinement indices for SmD_3 and $SmMg_2D_7$ (room temperature).

Crystal data		
empirical formula	SmD_3	$SmMg_2D_7$
M [g mol^{-1}]	156.40	213.07
crystal system	trigonal	tetragonal
space group	$P\bar{3}c1$ (no. 165)	$P4_12_12$ (no. 92)
a [pm]	653.9(1)[a]	624.10(1)[b]
c [pm]	676.7(2)[a]	934.81(2)[b]
V [10^6 pm^3]	250.5(1)	364.11(2)
Z	6	4
ρ_{calcd} [g cm^{-3}]	6.220	3.888
sample morphology	brown powder	light olive-green powder
Neutron powder diffraction		
λ [pm]	49.396(1)	
measurement range 2θ [°]	1.125–138.750	
step width ($\Delta 2\theta$) [°]	0.125	
measurement time [h]	10	9
Refinement		
program used for refinement	FullProf[19]	GSAS[20]
number of refined parameters	26	33
R_p	0.006	0.006
R_{wp}	0.009	0.007
R_{exp}	0.004	0.005
χ^2	4.1	2.6
R'_p [c]	0.065	0.007
R'_{wp} [c]	0.057	0.008
R_{Bragg}	0.036	0.046

[a] Hydride: $a = 656.7(3)$, $c = 680.1(3)$ pm. [b] Hydride: $a = 626.47(6)$, $c = 937.2(2)$ pm. [c] R'_p and R'_{wp} were calculated from background-corrected data.

Abstract in German: Binäres SmH_3 (trigonal, $a = 656{,}7(3)$, $c = 680{,}1(3)$ pm, $P\bar{3}c1$, $Z = 6$), ternäres $SmMg_2H_7$ (tetragonal, $a = 626{,}47(6)$, $c = 937{,}2(2)$ pm, $P4_12_12$, $Z = 4$) und die entsprechenden Deuteride (SmD_3: $a = 653{,}9(1)$, $c = 676{,}7(2)$ pm; $SmMg_2D_7$: $a = 624{,}10(1)$, $c = 934{,}81(2)$ pm) wurden durch Hydrierung (Deuterierung) von elementarem Samarium bzw. der Laves-Phase $SmMg_2$ dargestellt und mit Röntgen- bzw. Neutronenpulverbeugung und magnetischen Messungen (SQUID- und Vibrations-Magnetometer) charakterisiert. Das Problem der enormen Neutronenabsorption einer natürlichen Isotopenmischung ^{nat}Sm, wurde durch sorgfältige Wahl der Neutronenwellenlänge (≈ 50 pm), den Gebrauch doppelwandiger zylindrischer Probenträger und den Einsatz eines Hochfluss-Neutronendiffraktometers (D4c am ILL) umgangen. SmD_3 kristallisiert im Tysonit-Typ und hat drei unabhängige geordnete Deuteriumlagen mit trigonal-planarer, trigonal-pyramidaler und tetraedrischer Metallkoordination, wobei Sm-D-Bindungslängen im Bereich 220(1)–258(1) pm (im Mittel 235 pm) auftreten. $SmMg_2D_7$ ist ein neues Deuterid, das im $LaMg_2D_7$-Typ kristallisiert mit vier vollständig besetzten Deuteriumlagen mit trigonal-planarer und tetraedrischer Metallkoordination, wobei Sm-D-Bindungslängen im Bereich 227,6(5)–246,8(8) pm (im Mittel 239 pm) auftreten. Dies sind die ersten experimentell bestimmten Samarium-Deuterium-Bindungslängen in der Literatur. Beide Deuteride sind paramagnetisch bis 2 K (SmD_3: $\mu_{eff} = 0{,}63(1)\ \mu_B$, $\theta_p \approx -4$ K; $SmMg_2D_7$: $\mu_{eff} = 0{,}57(2)\ \mu_B$, $\theta_p \approx -4$ K). Kristallstruktur, chemische und physikalische Eigenschaften deuten auf vorwiegend ionische Wechselwirkungen gemäß der ionischen Grenzformeln $Sm^{3+}(H^-)_3$ und $Sm^{3+}(Mg^{2+})_2(H^-)_7$ hin.

conditions, with the lattice parameter a ranging from 862.74(1) pm for the samarium-rich to 863.39(2) pm for the magnesium-rich phase boundary. X-ray powder patterns for $SmMg_2H(D)_7$ could be indexed to a tetragonal cell (Table 1). The calculated patterns assuming an $LaMg_2D_7$-type structure show very good agreement with the patterns observed for $SmMg_2H_7$.

The complete crystal structure of SmD_3 was refined by the Rietveld method from neutron powder diffraction data (range: $5° \le 2\theta \le 85°$) using the program FullProf[19] (linear interpolation between 26 refined background points, refinement of scale factor, lattice, atomic, profile width u, v, w, pseudo-Voigt mixing and two asymmetry parameters). The program GSAS[20] was used for the Rietveld refinement of the crystal structure of $SmMg_2D_7$. The lattice parameters refined from X-ray powder diffraction data were kept fixed for the refinement from neutron powder diffraction data (range: $5° \le 2\theta \le 65°$). The following 33 parameters were allowed to vary during refinement: seven background (Chebyshev function), two scale factors, four profile parameters, 14 atomic coordinates and six thermal displacement parameters. Vanadium (sample holder) was taken into account as a secondary phase, for which only the scale factor was allowed to vary and profile parameters were constrained to be equal to those of the main phase for $SmMg_2D_7$. The refinement results with the neutron diffraction data corrected for absorption effects (program ABSOR[21]) do not differ significantly from those with uncorrected data for structural parameters. This is in agreement with a similar observation found for strongly absorbing europium deuterides.[13] The refined deuterium occupations do not deviate significantly from unity and were thus fixed at 1.0 for both SmD_3 and $SmMg_2D_7$. The observed and calculated patterns are shown in Figures 2 and 3, respectively, and the refined crystal structures are depicted in Figures 4 and 6 below. The refinement results and crystal structure data are summarised in Tables 1 and 2, respectively.

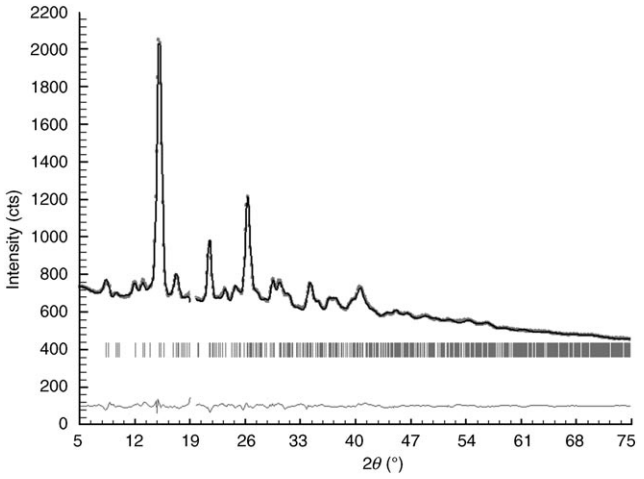

Figure 2. Observed (dotted line), calculated (solid line) and difference (bottom) neutron powder diffraction patterns of SmD_3 at room temperature (D4c,[22] $\lambda = 49.396(1)$ pm; excluded region: 19.25° to 19.75° in 2θ due to detector failure). Bragg markers indicate the positions of SmD_3 Bragg peaks. Intensity in total detector counts.

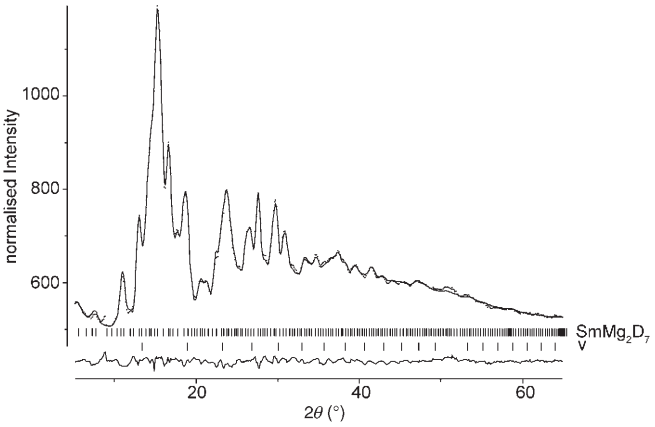

Figure 3. Observed (dotted line), calculated (solid line) and difference (bottom) neutron powder diffraction pattern of $SmMg_2D_7$ at room temperature (D4c,[22] $\lambda = 49.396(1)$ pm; excluded region: 19.375° to 19.625° in 2θ due to detector failure). Bragg markers indicate the positions of $SmMg_2D_7$ and V (sample holder) Bragg peaks. Intensity in total detector counts.

Table 2. Atom parameters of SmD_3 ($P\bar{3}c1$, no. 165) and $SmMg_2D_7$ ($P4_12_12$, no. 92). Form of the temperature factor: $\exp[-B_{iso}(\sin\theta/\lambda)^2]$.

SmD_3					
Atom	Site	x	y	z	B [10^4 pm^2]
Sm	6*f*	0.337(2)	0	1/4	0.86(8)
D1	12*g*	0.346(1)	0.319(1)	0.0845(7)	1.39(7)
D2	4*d*	1/3	2/3	0.186(1)	0.31(7)
D3	2*a*	0	0	1/4	2.0(3)
$SmMg_2D_7$					
Atom	Site	x	y	z	B [10^4 pm^2]
Sm	4*a*	0.2694(8)	x	0	0.79(8)
Mg	8*b*	0.0302(9)	0.251(1)	0.3469(6)	1.34(2)
D1	8*b*	0.038(1)	0.024(1)	0.1235(7)	2.84(8)
D2	8*b*	0.079(1)	0.4284(9)	0.1784(6)	2.13(8)
D3	8*b*	0.3133(9)	0.156(1)	0.2506(8)	1.97(8)
D4	4*a*	0.750(1)	x	0	2.4(2)

Discussion

Neutron absorption of samarium-containing compounds: Most elements have absorption cross-sections, σ_a, for thermal neutrons of the order of several barn (100 fm^2), which makes it possible to use rather large samples (typically cylindrical, with a diameter of 10 mm and a length of 50 mm) that are needed for neutron diffraction experiments to compensate for the moderate scattering cross-sections. Only four of the first 90 elements of the periodic table exhibit σ_a values above 1000 barn due to strong resonance for thermal neutrons, three of them being rare-earth metals. The values for natural isotopic mixtures listed for a wavelength of 179.8 pm are 2520 (Cd), 4530 (Eu), 5922 (Sm) and 49700 barn (Gd),[23] which seemingly make neutron diffraction experiments unfeasible. Owing to these extremely high values

these metals are used as neutron absorbers (cadmium as a shielding material for neutron sources and samarium and gadolinium in aqueous solutions as homogeneous neutron absorbers in nuclear fuel reprocessing).[24] A very elegant solution to the problem of neutron diffraction with highly absorbing materials is to use isotopically pure materials with a lower absorption cross-section, although this is generally prohibitively expensive for systematic studies of larger numbers of compounds. This method has been successfully employed for compressibility studies on $^{154}SmD_2$, although no structural parameters were reported.[9] We use a different approach, however, in which we optimise the experimental parameters by utilising the wavelength dependence of σ_a, which exhibits a strong resonance peak at around 95 pm for ^{nat}Sm (Figure 1). Unlike in the case of europium,[12] the minimum on the low-energy side of the resonance peak ($\lambda \approx 200$ pm) exhibits values well above 5000 barn, which is still much too high to be suitable for neutron diffraction. The only choice therefore seems to use very short wavelengths, which limits the expected resolution of the data as well as the number of neutron diffractometers available. Of these, we chose the high-intensity diffractometer D4c,[22] installed at the hot source at the Institut Laue-Langevin (Grenoble, France), which operates at $\lambda = 49.4$ pm. The neutron absorption cross-section of ^{nat}Sm at this wavelength is 187.3 barn (see Figure 1), which results in linear neutron absorption coefficients of 4.49 cm^{-1} for SmD_3 and 2.05 cm^{-1} for $SmMg_2D_7$. Thus, neutron diffraction can be considered feasible with a high-flux diffractometer and reduced sample thickness. The latter was realised by using double-walled vanadium cylinders in which the sample was placed only in the annular space between the outer and inner cylinders, thus maximizing the ratio of sample volume to sample thickness and minimizing the diffraction angle dependence of absorption effects at the same time (see Experimental Section).

The crystal structure of SmD_3: The structure of SmD_3 is essentially isotypic to that of its rare-earth congeners containing Nd–Lu (exceptions: Eu and Yb). This structure was originally established for HoD_3[25] and later refined for YD_3,[26] DyD_3[27] and NdD_3.[7] As shown in Figure 4, it displays a hexagonal close-packed (hcp) metal atom arrangement (Mg-type structure, layer A at $z = 1/4$, layer B at $z = 3/4$) in which deuterium fills one tetrahedral (D1) and two trigonal metal interstices (D2, D3). The deuterium in the latter two interstices is more or less displaced from its centre. The D sites are usually described by split atom positions but display essentially trigonal metal configurations (trigonal LaF_3-type structure). The atomic shifts induced by deuterium insertion lead to a tripling of the unit cell volume that can be visualised by using the concepts of group–subgroup relationships. In elemental samarium (hcp structure, Mg type), the atoms occupy the 2*c* position 1/3, 2/3, 1/4 in space group $P6_3/mmc$ (called "small cell" *a*, *b*, *c*). Tripling the unit cell (called "large cell" $a' = a - b$, $b' = a + 2b$, $c' = c$) in a klassengleiche symmetry reduction of index 3 leads to space group $P6_3/mcm$, which is followed by a translationengleiche reduction

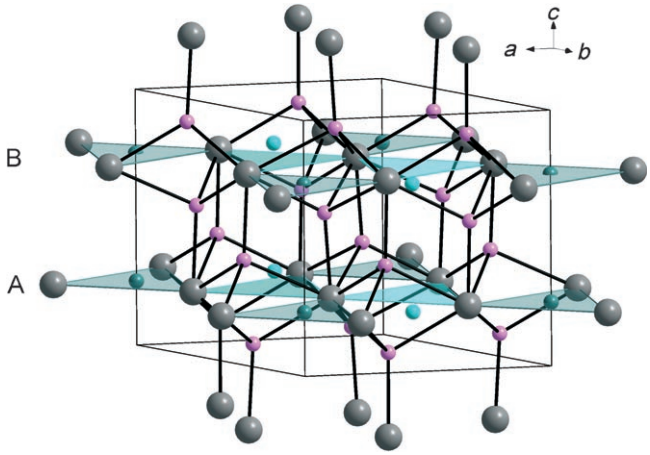

Figure 4. Crystal structure of SmD_3 with hexagonally close packed samarium atoms (layer notation AB). The tetrahedral arrangement of samarium atoms (large grey) around D1 atoms (pink) is shown. The shaded Sm_3 triangles represent the trigonal coordination of D2 (cyan) and D3 atoms (dark green). Note that D2 is significantly shifted from the triangle, whereas D3 is positioned within the triangular plane. See Table 3 for interatomic distances.

of index 2 to space group $P\bar{3}c1$, with corresponding metal atom positions 6*f* *x*, 0, 1/4 ($x = 1/3$). The coordinate observed for Sm ($x = 0.337(2)$) in SmD_3 does not deviate significantly from the ideal value ($x = 1/3$), which shows that the distortion of the metal matrix is negligible. This is not the case for the *c* axis, however, which is significantly elongated, as shown by the increased *c*/*a* ratio of 1.791 (small cell) compared to 1.633 in an ideal hcp structure. This is presumably due to the simultaneous occupancy of deuterium sites (D1) in neighbouring metal tetrahedra that share common faces perpendicular to the crystallographic *c* axis, as shown in Figures 4 and 5.

This is an unfavourable situation, according to Pauling's crystal chemical rules,[28] due to electrostatic repulsion between the deuteride anions, which presumably triggers the structural distortion observed in SmD_3, namely an elongation of the D1–D1 distance parallel to the crystallographic *c* axis from 157 to 227 pm. Other interatomic distances are listed in Table 3. This is manifested by an increased *c*/*a* ratio (see above) and a reduced *z* parameter for D1 (0.0845 in SmD_3 versus 0.125 for the centre of the tetrahedron), which at the same time makes the interlayer Sm–Sm distances (A–B is about 400 pm) considerably longer than the intralayer Sm–Sm distances (A–A and B–B are about 375 pm; see Figures 4 and 5). Two further crystallographically independent deuterium atoms occupy positions (D2, D3) with a nearly triangular coordination in an ordered manner. While D2 is clearly offset with respect to the coordination triangle of samarium atoms ($z = 0.184$ versus 1/4; see Figure 4) and shifted toward the centre of the adjacent octahedral void, D3, which is restricted by symmetry, is centred inside an Sm_3 triangle ($z = 1/4$), which results in a trigonal-planar coordination (Figure 4). Other interatomic distances are listed in Table 3.

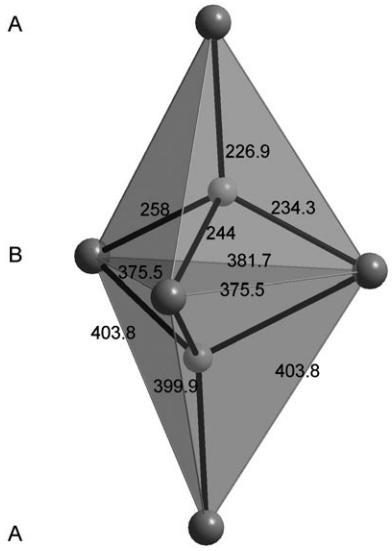

Figure 5. Face-sharing D1Sm$_4$ tetrahedra in the crystal structure of SmD_3. Interatomic distances (Sm–D in upper tetrahedron, Sm–Sm distances in lower tetrahedron and shared face) are given in picometres. Hexagonally close packed layers indicated by layer notation AB.

Table 3. Interatomic distances [pm] in SmD_3 and $SmMg_2D_7$.

	SmD_3		
Sm–D3	220(1)	D1–Sm	226.9(5)
Sm–D2 (×2)	221.1(6)	D1–Sm	234.3(9)
Sm–D1 (×2)	226.9(5)	D1–Sm	244(1)
Sm–D1 (×2)	234.3(9)	D1–Sm	258(1)
Sm–D1 (×2)	244(1)	D2–Sm (×3)	221.1(6)
Sm–D1 (×2)	258(1)	D3–Sm (×3)	220(1)
average Sm–D distance: 235			
shortest Sm–Sm contact: 376(1)			
shortest D–D contact (D1–D1): 226.0(7)			
	$SmMg_2D_7$		
Sm–D2 (×2)	227.6(5)	D1–Mg	185.4(9)
Sm–D1 (×2)	232(1)	D1–Sm	232(1)
Sm–D1 (×2)	240.4(9)	D1–Sm	240.4(9)
Sm–D2 (×2)	242.4(7)	D2–Mg	194.8(8)
Sm–D3 (×2)	246.2(8)	D2–Mg	220(1)
Sm–D3 (×2)	246.8(8)	D2–Sm	227.6(5)
Mg–D1	185.4(9)	D2–Sm	242.4(7)
Mg–D2	194.8(8)	D3–Mg	205.0(9)
Mg–D4	196.9(8)	D3–Mg	207(1)
Mg–D4	198.3(7)	D3–Sm	246.2(8)
Mg–D3	205.0(9)	D3–Sm	246.8(8)
Mg–D3	207(1)	D4–Mg (×2)	196.9(8)
Mg–D2	220(1)	D4–Mg (×2)	198.3(7)
average Sm–D distance: 239			
shortest Sm–Sm contact: 390.61(6)			
average Mg–D distance: 201			
shortest Sm–Mg contact: 338.1(9)			
shortest D–D contact (D1–D3): 224.9(7)			
shortest Mg–Mg contact: 307(1)			

The deuterium atom D3 exhibits a relatively high thermal displacement parameter (Table 2). The introduction of anisotropic thermal displacement parameters revealed a strong anisotropy along the crystallographic *c* axis perpendicular to the coordinating Sm_3 triangle. As expected, however, no reliable values could be determined. Although such behaviour may point to a static or dynamic disorder, refinements using split atom positions for that deuterium atom similar to those applied in NdD_3[7] did not improve the fit, nor did refining the D3 occupancy give any hints of non-stoichiometry. Another hint for a pronounced dynamic behaviour of hydrogen (deuterium) in this binary hydride (deuteride) is a considerable isotope effect with respect to the lattice parameters (*a* is 0.4 % and *c* 0.5 % smaller for the deuteride).

The gravimetric analysis of SmD_3 also favours a stoichiometric composition, therefore we can describe the crystal structure of samarium trideuteride as a trigonal LaF_3-type structure with a fully ordered deuterium distribution. The crystal structure, stoichiometry and colour of samarium trihydride (deuteride) suggest a saline character, in accordance with earlier investigations (heat capacity, inelastic neutron scattering experiments, theoretical calculations and measurements of the magnetic and electrical properties performed mainly on the hydride[29,30]).

The crystal structure of $SmMg_2D_7$: The ternary hydrides $LaMg_2H_7$, $CeMg_2H_7$[11] and $EuMg_2H_6$[12] have already been reported in studies on the hydrogenation behaviour of rare-earth/magnesium intermetallic compounds $LnMg_2$. In an older study the analogous Laves phase with samarium was reported to decompose into samarium hydride and magnesium metal under an atmosphere of 2 bar of hydrogen (temperature not given).[31] In contrast to these findings, we have now successfully synthesised a new compound, $SmMg_2H_7$, by hydrogenation (deuteration) of $SmMg_2$. $SmMg_2D_7$ crystallises in the acentric, non-polar crystal class 422 and is isotypic with $LnMg_2D_7$ (Ln = La, Ce).[11] Owing to the lanthanide contraction, the unit cell volume decreases in the series La (0.39110(3) nm^3[11]), Ce (0.38290(4) nm^3[11]) and Sm (0.36411(2) nm^3). Upon hydrogen (deuterium) uptake the cubic Laves phase (C15)-type intermetallic compound $SmMg_2$ ($a = 862.74$ pm, see above) undergoes a volume expansion by 13.4 % and a tetragonal distortion with $a' = a - b$, $b' = a + b$, $c' = c$ ($\Delta a/a = 2.4\,\%$, $\Delta c/c = 8.4\,\%$). The Sm–Sm distances in the diamond-like samarium sub-lattice expand from 373 to 391 pm in $SmMg_2D_7$, with a maximum deviation from the ideal tetrahedral angle of 7.7°. The tetrahedral Mg_4 framework suffers a more pronounced distortion, with the formerly uniform Mg–Mg distances now ranging from 307 to 347 pm and a tilting of the corner-sharing Mg_4 tetrahedra by 19.2° (see Figure 6). The intermetallic Sm–Mg distances range from 338 to 411 pm, with an average of 374.4 pm (357.5 pm in $SmMg_2$).

Thus, the crystal structure of $SmMg_2D_7$ can be described as a stuffed and distorted derivative of the cubic Laves phase (C15) type, in which deuterium occupies four crystallographically different types of interstices with trigonal or distorted tetrahedral metal environments. D1 is located almost exactly between two adjacent face-sharing [Sm_2Mg_2] tetrahedra and is only 6 pm above the coordinating [Sm_2Mg] triangle (185 pm from Mg (shortest metal–deuterium distance of the structure) and 232 and 240 pm from Sm; see

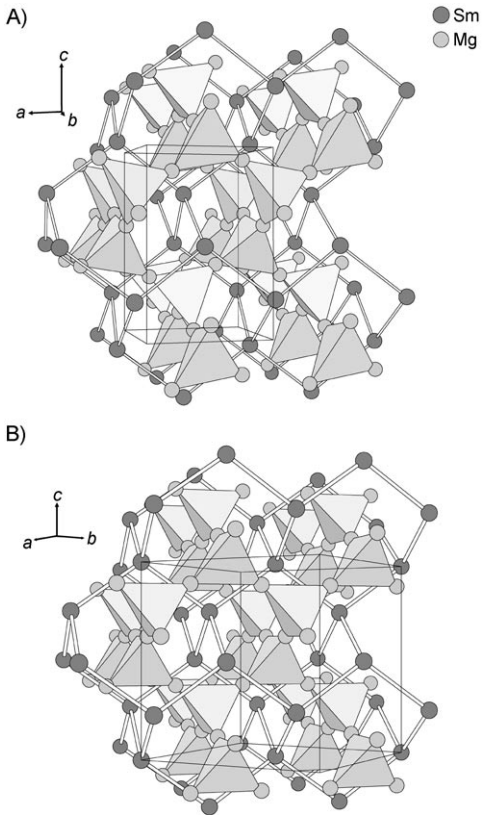

Figure 6. The metal atom substructure of $SmMg_2D_7$ (A) and the crystal structure of $SmMg_2$ (B) showing the unit cells.

Figure 7 and Table 3). The Mg atom that completes the tetrahedron is 253 pm from the deuterium and is therefore too far away to be included in the primary coordination sphere.

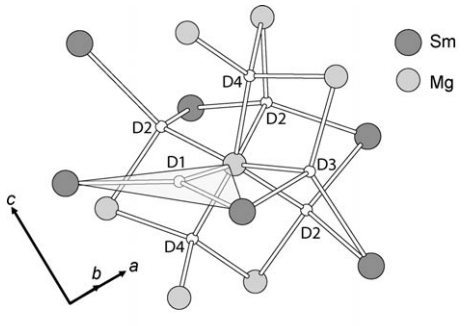

Figure 7. Coordination of deuterium by the metal atoms in $SmMg_2D_7$, with the trigonal surrounding of D1 shaded in grey.

The reason for this somewhat unusual D1 coordination might be the short D1–D1 contacts of about 200 pm in a hypothetical structure with D1 in regular tetrahedral interstices. Such an unfavourable repulsion is avoided by the observed shifting of D1 towards the [Sm_2Mg] triangle.

D2 and D3 occupy distorted [Sm_2Mg_2] tetrahedral voids at metal–deuterium distances ranging from 195 to 242 and 205 to 247 pm, respectively. D4 is located at the centre of an Mg_4 tetrahedron (197–198 pm) in a void that is rarely occupied in Laves phases. The mean Sm–D and Mg–D distances compare well with those in other Sm and Mg deuterides, such as SmD_3 (235 pm; see Table 3) and MgD_2 (195 pm).[32] Refinement of the deuterium occupancies did not deviate significantly from unity, therefore all deuterium positions are fully occupied, unlike in many other Laves phase hydrides. The coordination numbers of samarium and magnesium are 12 and 7, respectively, with strongly distorted polyhedra that are related to an anticuboctahedron and a monocapped trigonal prism, respectively.

Magnetic properties of SmD_3 and $SmMg_2D_7$: Both parent materials exhibit long range magnetic order. Sm orders antiferromagnetically below 109 K[33,34] and $SmMg_2$ shows a strong rise of the magnetisation in a narrow temperature range (between 26 and 50 K) just above the Neél temperature ($T_N = 26$ K),[35] which is not commonly associated with antiferromagnetic order and is thus a unique feature of this material. The temperature dependence of the magnetic susceptibility $\chi = M/H$ is plotted as $1/\chi$ versus T for SmD_3 and $SmMg_2D_7$ in Figures 8 and 9, respectively. These figures

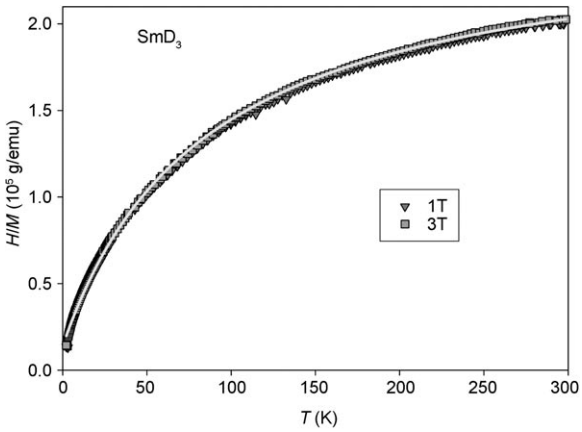

Figure 8. Inverse susceptibility of SmD_3 as a function of temperature for the indicated external fields. The solid line is a fit to the modified Curie–Weiss law.

demonstrate that both deuterides are paramagnetic down to 2 K. The full lines indicate the least-squares fit to the modified Curie–Weiss law $\chi = \chi_0 + C/(T - \theta_p)$, which includes the temperature-independent susceptibility χ_0. The Curie constant yields an effective moment μ_{eff} of 0.63(1) μ_B for SmD_3, which is below the theoretical value for that of the free Sm^{3+} state (0.845 μ_B). The negative paramagnetic Curie temperature, $\theta_p = -4(1)$ K, indicates antiferromagnetic correlations. The reduced effective moment as well as the significant curvature of $1/\chi(T)$ is typical for Sm compounds[36] and is due to crystal-field effects, which can be phenomenologically described by a temperature-independent susceptibility ($\chi_0 = 3.9 \times 10^{-6}$ emu g^{-1}).

In contrast to SmD_3, $SmMg_2D_7$ shows a pronounced field dependence of H/M (inverse susceptibility) which does not

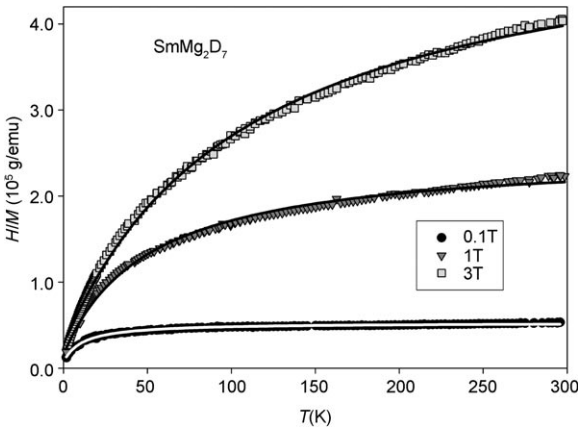

Figure 9. H/M (inverse susceptibility) of $SmMg_2D_7$ as a function of temperature for the indicated external fields. The solid line is a fit to the modified Curie–Weiss law.

diminish in high fields. The Curie–Weiss fit to these data yields an effective moment of 0.57(2) μ_B and a paramagnetic Curie temperature of $-4(1)$ K, while χ_0 is found to vary from 1.9×10^{-5} emu g^{-1} at 0.1 T to 3.8×10^{-6} and 1.9×10^{-6} emu g^{-1} at 1 and 3 T, respectively. Such a strong field-dependence is usually attributed to magnetic impurities or secondary magnetic phases. In this case, however, the strong field-dependence of M/H can be attributed to the unresolved amorphous secondary phase detected by X-ray diffraction, which yields different χ_0 values at different external fields. Nevertheless, we believe that the effective moment is intrinsic as the susceptibility data at various fields yield the same effective moment. To support this finding we reinvestigated the parent material with respect to possible magnetic impurity phases despite the fact that only a single report has appeared in the literature on the magnetic properties of $SmMg_2$.[35] Figure 10 shows the magnetisation of $SmMg_2$ at various fields, which is in good agreement with the data of Buschow et al.[35] From that, and the scaling of M/H above 50 K, we can conclude that the parent material contains no magnetic impurity phase and the above-mentioned unresolved amorphous phase must form during hydrogenation.

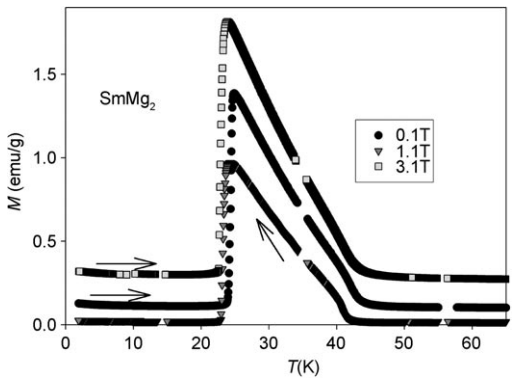

Figure 10. Magnetisation of $SmMg_2$ as a function of temperature for the indicated external fields. The arrows indicate the direction of temperature change.

This detailed re-investigation of $SmMg_2$ shows that the steep rise of the magnetisation below 41 K can be attributed to a weak ferromagnetic order of the small Sm moments, which yields a Curie temperature of 41 K. The antiferromagnetic transition at $T_N = 25$ K is a first-order phase transition associated with a temperature hysteresis of about 2 K. External fields shift the transition to lower temperatures, as is usual for antiferromagnetic order. For clarity, Figure 10 shows the magnetisation for 0.1 T on cooling and for 1 T and 3 T during warming only. As the antiferromagnetic transition occurs about 2 K lower on cooling than during warming, the 0.1-T measurement is situated just in between the 1-T and 3-T data. Further support for the first-order nature of the transition is obtained from magnetic isotherms: the magnetisation as a function of field for a second-order transition, plotted as M^2 versus H/M (Arrott plots), should give straight lines in the vicinity of T_c. This is reasonably well fulfilled in the vicinity of T_C ((41 ± 15) K). The magnetic isotherm at 22 K, however, yields an S-shape of the Arrott plot with a pronounced negative slope, which provides evidence for the first-order nature of the transition at $T_N = 25$ K. As can be seen from Figures 9 and 10, hydrogen absorption suppresses both the weak ferro- and the antiferromagnetic order.

To summarise, hydrogenation transforms the parent metal into a non-metal in both cases. Thus, long range magnetic order is suppressed to below 2 K in the non-metallic deuterides investigated since conduction electrons are necessary to mediate magnetic exchange interactions in terms of the RKKY exchange between the strongly localised 4f moments of Sm.

Conclusions

The crystal structures of SmH_3 (LaF_3 (tysonite) type) and of the new compound $SmMg_2H_7$ ($LaMg_2D_7$ type) have been determined by a combination of X-ray and neutron powder diffraction on the deuterides. Special care was taken to optimise the experimental conditions in view of the extremely high neutron absorption of the natural isotopic mixture of samarium, especially the choice of a short wavelength (ca. 50 pm), a reduction of the sample thickness (double-walled vanadium cans) and the use of a high-flux neutron diffractometer (D4c,[22] ILL, Grenoble). Despite the short wavelength and the still high neutron absorption, the Sm–D distances, which are reported for the first time, have been determined to an accuracy (esds of 1 pm or below) sufficient for a detailed crystal chemical discussion. A comparison with other rare-earth–deuterium distances reflects the lanthanide contraction. Thus, the mean Ln–D distances in the series of $LnMg_2D_7$ compounds vary from 247 pm (Ln = La)[11] to 244 (Ln = Ce)[11] and 239 pm (Ln = Sm). The mean interatomic distances between the lanthanide and fully occupied deuterium positions in the binary deuterides are also found to decrease with increasing atomic number of the lanthanide, from 243 pm in $LaD_{2.50}$[4] to 235 pm in $NdD_{2.27}$[37] and 235 pm in SmD_3. The unusual triangular coordination of

the deuterium atom D1 in $SmMg_2D_7$ (two Sm atoms at distances of 232 and 240 pm, respectively, and one Mg at 185 pm) is similar to that of D3 in SmD_3 and D(m1) in YD_3.[26] Interestingly, the mean metal–D1 distance of 219 pm is almost the same as the Sm–D3 distance in SmD_3 (220 pm). Its crystal structure, chemical and magnetic properties and colour suggest that $SmMg_2D_7$ is a salt-like semiconducting metal hydride. The same is true for $LaMg_2H_7$ and $CeMg_2H_7$, for which a band gap of 2.6 eV has been calculated.[38] Thus, such compounds may be described by an ionic limiting formula of $Ln^{3+}(Mg^{2+})_2(H^-)_7$ (Ln = La, Ce, Sm). In contrast to the parent metal and intermetallic compound, both SmD_3 and $SmMg_2D_7$ are paramagnetic down to 2 K, in other words long-range magnetic order is suppressed, since the conduction electrons necessary for the propagation of magnetic interactions by the RKKY mechanism are lacking in the non-metallic deuterides.

Experimental section

The starting materials were samarium ingot (natural isotopic mixture, Ames Laboratory, 99.996 %), magnesium pieces (United Minerals, 99.995 %), hydrogen gas (Carbagas, 99.9999 %) and deuterium gas (AGA, 99.8 %). All handling of materials was carried out in an argon-filled glove box. Binary samarium trihydride (deuteride) was prepared by direct hydrogenation (deuteration) of samarium metal pieces in an iron crucible inside an autoclave. The reaction was performed at 700 K and a hydrogen (deuterium) gas pressure of 30 bar for two days. The reaction product consisted of dark grey pieces with a metallic lustre that could easily be ground into a brown powder. Gravimetric analysis of the deuterium uptake yielded the composition $SmD_{3.02(1)}$. Synthesis of the ternary samarium magnesium hydride (deuteride) was attempted by hydrogenation (deuteration) of a series of intermetallic compounds having the compositions SmMg, $SmMg_2$, $SmMg_3$, $SmMg_5$ and Sm_5Mg_{41}. The alloys were prepared either by arc melting or by reaction of the metals in sealed tantalum containers enclosed in sealed silica tubes. Suitable heat-treatment procedures were determined from a published Sm-Mg phase diagram.[18] The samples were ground into powders and placed in iron crucibles inside an autoclave in which the hydrogen (deuterium) pressure was slowly increased (20 bar per hour or less). Reaction at 100 bar of hydrogen (deuterium) pressure and 600 K during ten days yielded mixtures of binary samarium and magnesium hydrides for all compositions. Reaction of the samples SmMg and $SmMg_2$ under 128 bar of hydrogen (deuterium) pressure at 400 K for two days yielded a new olive-green phase, later found to be $SmMg_2H_7$, while the samples $SmMg_3$, $SmMg_5$ and Sm_5Mg_{41} decomposed into mixtures of binary samarium and magnesium hydrides. $SmMg_2D_7$ was synthesised by deuteration of $SmMg_2$ powder for two days at 420 K and a pressure of 145 bar. Contrary to the phases $LnMg_2$ (Ln = La, Ce), which start to absorb hydrogen at room temperature,[11] the reaction did not commence below about 390 K. As shown by X-ray powder diffraction, the compound was single phase with some amorphous content. The non-metallic character of the sample was confirmed by measuring its electric resistance, which was found to be very high. In contrast to SmH_3, which decomposes rapidly into $Sm(OH)_3$ (the deuterides react the same) upon contact with air, $SmMg_2H(D)_7$ turned out to be stable, at least for a few weeks.

The reaction products were examined by X-ray powder diffraction on a Guinier camera (samples enclosed in sealed glass capillaries of 0.3-mm outer diameter, $Co_{K\alpha1}$ radiation, internal silicon standard) or on Bragg-Brentano diffractometers (Philips PW1820, $Cu_{K\alpha1,2}$ radiation, internal silicon standard; Bruker D8 Advance, $Cu_{K\alpha1}$ radiation), with flat sample holders for air-sensitive substances. Neutron powder diffraction data were recorded at the high intensity diffractometer D4c[22] at ILL (Grenoble, France) equipped with a position-sensitive detector. In order to reduce the absorption the samples (2.790 g of SmD_3 and 1.495 g of $SmMg_2D_7$ powders, respectively) were filled into double-walled vanadium cylinders (length: 64 mm; inner diameter of the outer tube: 9.15 mm; annular sample thickness: 0.6 mm; hermetically sealed with an indium wire). The wavelength and zero point of the neutron diffractometer were determined with a standard nickel sample to be 49.396(1) pm and 0.1060(6)°, respectively, and were kept fixed during subsequent refinements. Diffraction data were taken at room temperature in the range $1.125 \le 2\theta \le 138.750°$ ($\Delta 2\theta = 0.125°$) during total data collection times of 10 and 9 h for SmD_3 and $SmMg_2D_7$, respectively. Further details of the crystal structure investigations may be obtained from Fachinformationszentrum Karlsruhe, 76344 Eggenstein-Leopoldshafen, Germany (fax: (+49) 7247-808-666; e-mail: crysdata@fiz-karlsruhe.de) on quoting the deposition numbers CSD-416785 and CSD-416845 for SmD_3 and $SmMg_2D_7$, respectively.

Magnetic measurements were performed on both the deuterides and a binary intermetallic sample ($SmMg_2$) with commercial SQUID and vibration magnetometers (Cryogenics Ltd. and Quantum Design, respectively) in the temperature range from 2 K to room temperature and in fields up to 6 and 9 T, respectively. The measurements on the metallic $SmMg_2$ were performed on bulk 20-mg specimens and on powders of the deuterides of about 4 mg which were encapsulated in quartz capillaries as sample holders.

Acknowledgement

We thank Pierre Palleau (D4c at the ILL, Grenoble) for technical assistance during the neutron diffraction experiments. This work was supported by the Swiss National Science Foundation, the German National Science Foundation and the Swiss Federal Office of Energy.

[1] L. Schlapbach, *MRS Bull.* **2002**, 675–679.
[2] P. Vajda in *Handbook on the Physics and Chemistry of Rare Earths, Vol. 20* (Eds.: K. A. Gschneidner, Jr., L. Eyring), Elsevier, New York, **1995**, pp. 207–291.
[3] K. Yvon, B. Bertheville, *J. Alloys Compd.* **2006**, *425*, 101–108.
[4] T. J. Udovic, Q. Huang, J. J. Rush, *J. Solid State Chem.* **1996**, *122*, 151–159.
[5] J. Schefer, P. Fischer, W. Haelg, J. Osterwalder, L. Schlapbach, J. D. Jorgensen, *J. Phys. C* **1984**, *17*, 1575–1583.
[6] G. Renaudin, P. Fischer, K. Yvon, *J. Alloys Compd.* **2002**, *330–332*, 175–178.
[7] G. Renaudin, P. Fischer, K. Yvon, *J. Alloys Compd.* **2000**, *313*, L10–L14.
[8] C. E. Holley, Jr., R. N. R. Mulford, F. H. Ellinger, *J. Phys. Chem.* **1955**, *59*, 1226–1228.
[9] I. N. Goncharenko, V. P. Glazkov, O. A. Lavrova, V. A. Somenkov, *Sov. Phys. Solid State* **1992**, *34*, 1585–1586.
[10] O. Greis, P. Knappe, H. Müller, *J. Solid State Chem.* **1981**, *39*, 49–55.
[11] F. Gingl, K. Yvon, T. Vogt, A. Hewat, *J. Alloys Compd.* **1997**, *253–254*, 313–317.
[12] H. Kohlmann, F. Gingl, T. Hansen, K. Yvon, *Angew. Chem.* **1999**, *111*, 2145–2147; *Angew. Chem. Int. Ed.* **1999**, *38*, 2029–2032.
[13] H. Kohlmann, K. Yvon, *J. Alloys Compd.* **2000**, *299*, L16–L20.
[14] H. Kohlmann, K. Yvon, Y. Wang, *J. Alloys Compd.* **2005**, *393*, 11–15.
[15] M. Bortz, M. Gutmann, K. Yvon, *J. Alloys Compd.* **1999**, *285*, L19–L21.
[16] J. E. Lynn, P. A. Seeger, *At. Data Nucl. Data Tables* **1990**, *44*, 191–207.
[17] "Hydrides": G. G. Libowitz, A. J. Maeland in *Handbook on the Physics and Chemistry of Rare Earths, Vol. 3* (Eds.: K. A. Gschneidner, Jr., L. Eyring), North-Holland, **1979**, pp. 299–336.

[18] A. Saccone, S. Delfino, G. Borzone, R. Ferro, *J. Less-Common Met.* **1989**, *154*, 47–60.
[19] J. Rodríguez-Carvajal, FullProf.2k, Version 2.70, **2004** (LLB, unpublished).
[20] A. C. Larson, R. B. Von Dreele, General Structure Analysis System (GSAS), Los Alamos National Laboratory Report LAUR 86-748, **2000**.
[21] D. Schmitt, B. Ouladdiaf, *J. Appl. Crystallogr.* **1998**, *31*, 620–624.
[22] H. E. Fischer, G. J. Cuello, P. Palleau, D. Feltin, A. C. Barnes, Y. S. Badyal, J. M. Simonson, *Appl. Phys. A* **2002**, *74*, S160–S162.
[23] V. F. Sears, *Neutron News* **1992**, *3*, 26–37.
[24] E. V. Renard, *Atomanya Energiya* **1992**, *72*, 444–451.
[25] M. Mansmann, W. E. Wallace, *J. Phys.* **1964**, *25*, 454–459.
[26] T. J. Udovic, Q. Huang, J. J. Rush, *J. Phys. Chem. Solids* **1996**, *57*, 423–435.
[27] T. J. Udovic, Q. Huang, J. W. Lynn, R. W. Erwin, J. J. Rush, *Phys. Rev. B* **1999**, *59*, 11852–11858.
[28] L. Pauling, *The Nature of the Chemical Bond and the Structure of Molecules and Crystals*, 3rd ed., Cornell University Press, Ithaca, **1960**.
[29] H. Bergmann, *Gmelin Handbuch der Anorganischen Chemie, Seltenerdmetalle Teil C1, Sc, Y, La und Lanthanide*, Springer, Berlin, **1974**, p. 1.
[30] W. E. Wallace, S. K. Malik, T. Takeshita, *J. Appl. Phys.* **1978**, *49*, 1486–1491.
[31] R. L. Beck, W. M. Mueller, U.S. Atomic Energy Commission Report, Contract No. AT(33-3)-3, **1962**.
[32] W. H. Zachariasen, C. E. Holley, J. F. Stamper, Jr., *Acta Crystallogr.* **1963**, *16*, 352–353.
[33] S. Legvold, *Rare Earth Metals and Alloys in Handbook on Ferromagnetic Materials, Vol. 9* (Ed.: E. P. Wohlfarth), North Holland, Amsterdam, **1980**, p. 183.
[34] K. A. Mc Ewen, P. F. Touborg, G. J. Cock, L. W. Roeland, *J. Phys. F: Met. Phys.* **1974**, *4*, 2264.
[35] K. H. J. Buschow, R. C. Sherwood, F. S. L. Hsu, *J. Appl. Phys.* **1978**, *49*, 1510–1512.
[36] M. Vybornov, W. Perthold, H. Michor, T. Holubar, G. Hilscher, P. Rogl, P. Fischer, M. Divis, *Phys. Rev. B* **1995**, *52*, 1389–1404.
[37] G. Renaudin, P. Fischer, K. Yvon, *J. Alloys Compd.* **2001**, *329*, L9–L13.
[38] E. Orgaz, *J. Alloys Compd.* **2001**, *322*, 45–54.

Received: May 26, 2006
Revised: November 14, 2006
Published online: January 17, 2007

